

Measurements and modelling of axial emission profiles in abnormal glow discharges in argon: heavy-particle processes

D Marić¹, P Hartmann², G Malović¹, Z Donkó² and Z Lj Petrović¹

¹ Institute of Physics, POB 68, 11080 Zemun, Belgrade, Serbia and Montenegro, Yugoslavia

² Research Institute for Solid State Physics and Optics, Hungarian Academy of Sciences, POB 49, H-1525 Budapest, Hungary

Received 15 July 2003

Published 15 October 2003

Online at stacks.iop.org/JPhysD/36/2639

Abstract

We report studies on argon glow discharges established between flat disc electrodes, at pressure \times electrode separation (pd) values between 45 and 150 Pa cm, with special attention to heavy-particle processes including heavy-particle excitation induced light emission. The discharges are investigated experimentally and also through self-consistent hybrid modelling. The comparison of the experimental and computed light intensity distributions verifies the correctness of the model, which gives a detailed insight into the discharge operation. The efficiency of heavy-particle excitation shows a universal dependence on the reduced electric field. At the higher pd values the scaling of electrical characteristics and light emission intensity with electrode separation is verified, however, additional processes (radial losses of charged particles and reduction of the active cathode area) result in the violation of scaling at the lowest pd value when the discharge tube diameter is kept constant.

1. Introduction

Recently, a series of papers have appeared that promised to carry out a systematic revision of Townsend's theory of gas breakdown [1–3]. While most of the elements of this work have been present in other studies, this has been a comprehensive attempt based on quantitative comparisons with well-defined experimental data. It has been found that in the low current limit the secondary electrons are produced mainly by photons at low E/N (reduced electric field) and heavy-particle ionization of gas atoms at high E/N , while ions play a dominant role only for intermediate values of E/N . It has also been found that metastables have observable contribution at all E/N . Including all these processes [3] with appropriate experimental collision data came close to actually reconciling the results for secondary yields obtained in beam experiments and by analysis of the Paschen curve or other gas discharge techniques. For the low current limit, fluxes of particles reaching the cathode are proportional to the

flux of electrons (at the anode) so it was possible to assign effective secondary yield associated with the ion flux and obtain consistent results from swarm experiments. However, such an approach may not function for higher current, normal glow, abnormal glow, rf and other discharges. That is due to several possible effects. First, spatial distribution of emission is quite different from that in Townsend discharges. Since the spatial emission profile consists of the cathode fall that is mostly dark and where electrons are in non-equilibrium, of a negative glow where field is close to zero but emission and ionization are at maximum and other regions which may or may not exist, it is quite possible that the flux of photons at the cathode will have a complex behaviour as a function of electron current and thus the proportionality between two fluxes would be broken, or at least depend on other properties of the discharge. On the other hand, even the ions that cross the cathode fall and reach the cathode may have their energy strongly affected by the general parameters of the discharge. One example of the failure to achieve linear conditions and

thus employ effective secondary yield associated with the ions is the situation when the ratio of the length and the width of the discharge tube becomes large and thus the solid angle of photon losses increases. In such a case, classic pd scaling (where p is the pressure and d is the electrode gap) may be broken. Under similar circumstances (i.e. when the ratio is large) it has been considered that the scaling may break down due to loss of electrons in radial direction [4], however, in that case the walls should have a large conductivity or a radial field partially blocking the flow of electrons is formed. A study with discharge tubes with conducting walls indicated that a significant increase of the discharge voltage accompanies the reduction of the tube diameter [5]. The violation of the $U = f(j/p^2)$ scaling (where U is the discharge voltage and j is the current density) was primarily attributed to the decrease of the active part of the cathode surface, due to the specific electric field distribution at the edges of the cathode.

Most of the models of gas discharges and plasmas consider only ion-induced secondary electrons—this approach cannot be regarded as correct for most of the conditions [3]. Attempts have been made to use volt–ampere characteristic [6] and spatial emission profiles [7] to provide effective secondary electron yields. These results, as expected, were different from the effective yield data obtained for the low current limit. Excellent internal consistency between spatial profiles and relative emission intensities has been obtained between a one-dimensional model and experimental data for the abnormal glow for almost all conditions covered by Marić *et al* [7].

The aim of this work is to explore the main mechanisms that give rise to the general behaviour of abnormal glow discharges characterized by the significant increase of voltage with increasing current, followed by a gradual decrease of the cathode-fall thickness. This kind of behaviour can arise due to various processes in the discharge such as redistribution of charged species, space-charge effects, gas and electrode heating, excited molecules and stepwise processes, electron and ion recombination, heavy-particle collisions. Any comparison between experiment and theory would be inadequate if the discharge operates under conditions where all of these processes are active. Therefore, we try to identify the conditions where the basic space-charge effects dominate and where possibly few more processes are gradually included—in order to observe how they manifest to the results of the measurements. The abnormal glow discharge is the primary subject of this investigation as the simplest mode of the glow discharge as compared to the constricted glow discharge, which would require development of a more complex two-dimensional model. On the other hand, we exclude the range of very high currents where heating of the cathode could introduce additional non-linear effects, which would further complicate modelling of the discharge.

It has been shown that space-charge dominated discharges follow E/N , pd and j/p^2 scaling derived from simple models (e.g. [8]). As certain processes in the discharge would cause breakdown of such scaling, systematic measurements of discharge parameters and spatial emission profiles, covering a wide range of discharge conditions, along with the application of the simple scaling laws, provide us with a useful diagnostic tool.

We have already reported studies of the voltage–current characteristics and axial light emission profiles of argon glow

discharges with plane-parallel electrodes [7]. This previous work has covered the normal to moderately abnormal current range, where excitation of the gas atoms primarily occurs via electron impact excitation. The discharges have also been described by a one-dimensional ion–electron hybrid model. An excellent agreement was obtained between the experimental data and the results of the simulations in terms of the axial emission profiles, proving the correctness of the model. The model also made it possible to determine the apparent secondary electron yield for a wide range of operating conditions, by taking the measured electrical data as input parameters of the simulations. The apparent electron yield data as a function of the reduced electric field at the cathode were found to agree reasonably with the results of previous calculations [9]. In [7], we have studied the range of applicability of the one-dimensional model: the only mismatch between the axial profiles that we have found occurred for the highest pd value where constriction of the discharge was significant at low currents. The simulations presented in [7] indicated the existence of an electric field reversal. The position of the field reversal point was found to be in excellent agreement with the predictions of the analytical model of [10]. Finally, in addition to the more extensive comparisons of the hybrid model with experimental data, strong support was given to the usual assumption that the position of the peak of emission coincides with the edge of the cathode-fall region.

This paper reports further studies of light emission, with special attention devoted to the excitation due to heavy particles (especially fast atoms). Heavy-particle processes become important at high E/N . These conditions may be achieved at low pd values where the increased discharge voltage results in high E/N , which favours excitation by heavy particles. Investigations by Phelps and Petrović have shown that in the case of homogeneous electric field (i.e. in the Townsend discharge regime) in argon gas, these processes are very important at E/N values in excess of ≈ 10 kTd. Studies of the breakdown in helium gas have shown that heavy-particle processes are indeed responsible for the special shape of the Paschen curve of helium [11]. While these previous studies considered the case of homogeneous field, the effects of heavy-particle processes (contribution to the production of ions and metastable atoms, and to spectral line excitation) in glow discharges with well-developed cathode sheath region have been studied by Bogaerts *et al* [15–17]. This work also focuses on discharges operating under such conditions. To achieve the conditions where heavy-particle processes play an important role, the operating conditions are shifted to higher currents with respect to those presented in [7]. These experimental studies of the discharges are also complemented by discharge simulations based on a comprehensive model that includes the transport and collision processes of fast heavy particles.

Section 2 of this paper describes the experimental set-up, while the simulation model is outlined in section 3. Section 4 presents the experimental and modelling results, and their comparison. The summary of the work is given in section 5.

2. Experimental

The schematics of the experimental set-up (as described in the previous paper [7]) is shown in figure 1. The discharge tube

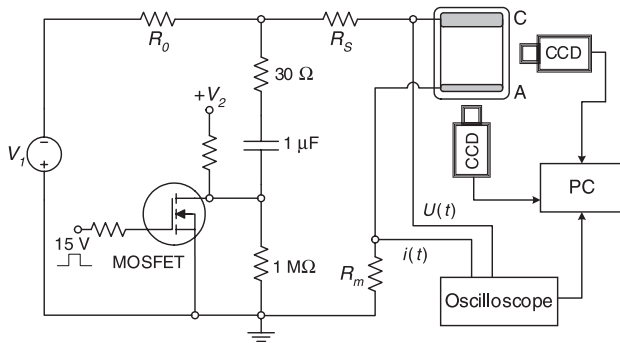


Figure 1. Simplified schematics of the experimental set-up and the electrical circuit.

consists of parallel plane electrodes inside a quartz cylinder that prevents the long-path breakdown. The cathode (C) is made of copper and the anode (A) of quartz with a transparent yet conductive thin film of platinum deposited on its surface facing the discharge. The diameter of the electrodes ($2r$) is 5.4 cm while the electrode separation (d) can be fixed at three different values (1.1, 2.1 and 3.1 cm).

The system is pumped down to a base pressure of the order of 10^{-6} Torr. Operating pressure is achieved by using a very small flow of pure argon. Before the measurements, the surface of the cathode is treated by a relatively high current discharge in hydrogen ($30 \mu\text{A}$) until a stable breakdown voltage is achieved.

The volt–ampere characteristic of the discharge is scanned by applying a pulse of current in addition to a very small dc current (typically $1\text{--}2 \mu\text{A}$) [12, 13]. This way it is possible to avoid heating and significant conditioning of the cathode during the measurements and to obtain reproducible results. Pulses of higher current last long enough to make a reliable recording of voltage and current transients. At the same time, the axial intensity profiles are recorded by a CCD camera so that the emission profiles correspond to the conditions of the pulse, not to the dc current.

Besides the measurement of the volt–ampere curves of the discharges and the axial emission profiles, we also measure radial profiles of emission through the transparent anode electrode to obtain information about the radial structure of the discharge. Recordings of axial and radial emission profiles are made by a cooled CCD camera sensitive mostly in the red part of the spectrum. While we do not measure absolute values of the intensity, relative relationship between the emission profiles at different currents is established by making recordings under identical conditions for two different openings of the aperture. Thus, we can be sure that the recorded emission signal is not saturated and we maintain the relative calibration. In principle, it is possible to make absolute calibration by normalizing the profiles in the low current Townsend regime to excitation coefficients at the anode.

Measurements are made in pure argon at pressure (p) \times gap (d) products of $pd = 150 \text{ Pa cm}$, 75 Pa cm and 45 Pa cm , at gap values 1.1 cm, 2.1 cm and 3.1 cm, respectively.

3. Simulation model

The simulations are based on a hybrid model [14, 15, 18–24] that combines the fluid description of argon ions and slow

electrons with kinetic description of fast plasma species: fast electrons, argon ions and fast neutral atoms. The non-hydrodynamic transport of the fast species in the discharge requires a kinetic approach [25]: use of particle simulation techniques [26, 27] or the solution of the Boltzmann equation [28–33]. Due to its flexibility and easier handling we chose Monte Carlo (MC) simulation for this purpose. For the slow electrons that are no longer able to ionize the gas, the hydrodynamic treatment is sufficiently accurate, so these electrons can be described by a computationally more effective fluid model. In this model, we use the usual way to distinguish between fast and slow electrons (based on their ability to excite the gas) [34, 35]. We also describe the motion and collision processes of argon ions (Ar^+) and fast neutral atoms (Ar^f) in the cathode sheath by MC simulation. The simulation of the fast heavy particles allows us to consider elementary processes, e.g. heavy-particle induced excitation and ionization, which are often neglected in discharge models.

In hybrid models, the ‘apparent’ secondary electron emission coefficient $\gamma = (j^-/j^+)_{\text{cathode}}$ (i.e. the ratio of the electron current to the ion current at the cathode) is usually defined as an input parameter. It is usually quite difficult to choose γ in a proper way due to the lack of data in the literature for cathode surfaces under discharge conditions. Thus, most of the models use a constant value for γ , even for a wide range of discharge conditions. Recent studies have, however, shown that γ may depend considerably on the actual discharge conditions [3, 6, 24, 36]. Because of this, in this model γ is taken as a variable (fitting) parameter and in the iterative solution of the fluid and MC models γ is adjusted ‘automatically’ to obtain a current density converging to the experimental value [37, 38].

As a check of the γ values obtained through the above fitting procedure, we also calculate the secondary electron yield from the energy-dependent secondary electron yield data ($\gamma_i(\varepsilon)$ and $\gamma_a(\varepsilon)$) characteristic for fast ions and atoms:

$$\gamma_{\text{calc}} = \frac{\sum_{k=1}^{N_i} \gamma_i(\varepsilon_k) + \sum_{k=1}^{N_a} \gamma_a(\varepsilon_k)}{N_i}, \quad (3.1)$$

where N_i and N_a , respectively, denote the number of ions and fast atoms arriving to the cathode in the MC cycle [24, 39]. The data for $\gamma_a(\varepsilon)$ and $\gamma_i(\varepsilon)$ are taken from [3]; they characterize ‘practical’ or ‘dirty’ cathode surfaces for which the electron yields can be significantly different compared to those obtained using ion beam experiments with heavily sputtered samples in ultrahigh vacuum environment.

The basic motivation of these modelling studies is to reproduce the experimentally observed excitation profiles in the abnormal glow operation mode of the discharge. As in the abnormal mode the current density distribution over the cathode is nearly uniform, a one-dimensional model can provide sufficient accuracy for our purposes, as it has already been demonstrated in the earlier work [7] where (at current densities lower compared to those in this work) we have obtained excellent agreement between measured light intensity profiles and those calculated from a one-dimensional hybrid model. The one-dimensional model, on the other hand, cannot directly account for the mechanisms (e.g. radial losses of charged particles) found responsible for the violation of scaling in this experimental work. The effects of these processes on the spatial distribution of the light intensity can be,

however, implicitly taken into account in the one-dimensional model through the increased discharge voltage determined experimentally.

While this model is one-dimensional in space, the MC part of the model is three-dimensional in velocity space. The fluid equations are solved on a uniform grid containing 300 points (i.e. with a resolution $\Delta x = d/300$). The boundary conditions at the walls are zero density of particles and prescribed values of the potential (zero at the cathode and V at the anode). The fluid equations are solved using an implicit integration scheme [40] with a typical integration time step of the order of 10 ns.

In these calculations, we assume that the spatial distribution of the light intensity is proportional to the electron impact or heavy-particle impact excitation rate, calculated from the MC routines in the following way.

In the MC simulation, the number of excitation events caused by different particles is counted at different spatial positions. The positions of individual excitation events are assigned to the points of a grid (which has the same Δx resolution as the one used in the fluid model). If $N_e(x_k)$ is the number of electron impact excitation events that have occurred near $x_k = k\Delta x$, due to the emission of N_0 primary electrons from the cathode, the excitation rate at that position is given by (see, e.g. [22]):

$$S_e(x_k) = \frac{j}{e(1+1/\gamma)\Delta x} \frac{N_e(x_k)}{N_0}, \quad (3.2)$$

where j is the current density. The excitation rates due to fast atom impact ($S_a(x_k)$) and ion impact ($S_i(x_k)$) are calculated in exactly the same way, from the corresponding $N_a(x_k)$ and $N_i(x_k)$ distributions.

3.1. The fluid model

The fundamental quantities in the one-dimensional fluid model are the electric potential and the density of slow electrons and Ar^+ ions. Particle balance for these species is expressed by the continuity equations:

$$\begin{aligned} \frac{\partial n_e}{\partial t} + \frac{\partial \phi_e}{\partial x} &= S_e, \\ \frac{\partial n_i}{\partial t} + \frac{\partial \phi_i}{\partial x} &= S_i, \end{aligned} \quad (3.3)$$

where n_e and n_i are the electron and ion densities, ϕ_e and ϕ_i are the electron and ion fluxes and S_e and S_i are the source functions of slow electrons and Ar^+ ions, respectively. The fluxes are calculated on the basis of the drift-diffusion approximation:

$$\begin{aligned} \phi_e &= -\mu_e n_e E - \frac{\partial(n_e D_e)}{\partial x}, \\ \phi_i &= \mu_i n_i E - \frac{\partial(n_i D_i)}{\partial x}, \end{aligned} \quad (3.4)$$

where μ_e and μ_i are the mobilities of electrons and ions, respectively. $E = -\partial V/\partial x$ is the x component of the electric field and V is the potential:

$$\frac{\partial^2 V}{\partial x^2} = -\frac{e}{\epsilon_0}(n_i - n_e), \quad (3.5)$$

where e is the elementary charge and ϵ_0 is the permittivity of free space. The diffusion coefficients D_e and D_i are calculated from the Einstein relation: $D = \mu k_B T$ where k_B is the Boltzmann constant and T is the characteristic energy for the given species. In these calculations we take $k_B T_e = 1$ eV [14, 15, 19, 35, 41] and $k_B T_i = 0.026$ eV. The mobility of electrons is given by $\mu_e = 3 \times 10^5/p$ cm² V⁻¹ s⁻¹ with p given in Torr, and the Ar^+ ion mobility, μ_i , as a function of E/N is taken from [3].

The ionization source function $S_i(x)$ is accumulated from the individual ionization processes in the MC routine, by summing contributions of different channels (electron, ion and fast atom impact ionization events). The electrons are transferred to the slow electron group (through the $S_e(x)$ source function) when their (kinetic + potential) energy falls below the excitation energy of the argon atoms.

3.2. The MC model

The motion of energetic particles is traced using MC simulation. In this algorithm random numbers are used to determine the positions and the types of the collisions.

Electrons are traced by MC simulation from the moment of their ‘creation’ (emission from the cathode or ejection from an atom’s shell in ionization) until (i) their total (kinetic + potential) energy falls below the first excitation energy of the gas, or (ii) they reach the anode. For the primary electrons backscattered to the cathode we take into account elastic and inelastic reflection/re-emission [43] and absorption at the cathode. Energetic electrons hitting the anode can be absorbed or reflected and can initiate secondary electron emission.

Positive ions and fast neutral atoms (Ar^f) in the cathode sheath are traced (i) until they reach the cathode, or (ii) in the case of the fast atoms, their energy falls below an energy limit (0.01 eV) that is used to distinguish between fast and thermal atoms. Fast heavy particles that reach the cathode surface can be absorbed or reflected with a certain probability and with a fraction of their kinetic energy [24, 44].

3.3. Elementary processes

The elementary processes considered in the MC submodels for electrons, positive ions and fast atoms include elastic scattering of the projectiles, as well as excitation and ionization of Ar atoms by the projectiles. The cross sections of elementary processes are taken from Phelps [45–47] and are displayed in figure 2.

The scattering of electrons in elastic momentum transfer and excitation collisions is assumed to be isotropic. In the case of electron impact ionization, the energies of the scattered and ejected electrons, and the directions of their velocity vectors are calculated in accordance with the procedures described in [27, 48, 49].

The cross section of the isotropic part of the elastic $\text{Ar}^+ + \text{Ar}$ collisions (Q_i) is taken from [47], while the charge transfer cross section (backward part of elastic scattering, Q_b) is obtained from the momentum transfer cross section (Q_m) as $Q_b = (Q_m - Q_i)/2$, as explained in [47]. In isotropic collisions, the scattering and azimuth angles are chosen to reflect isotropic scattering in the centre-of-mass (COM)

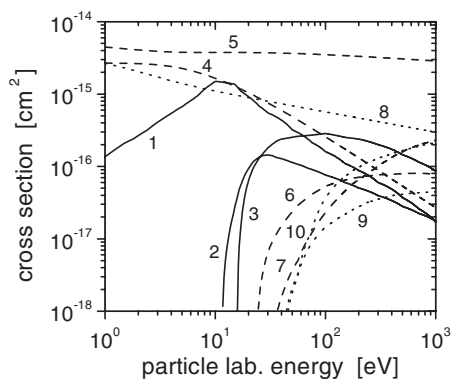


Figure 2. Cross sections of the elementary processes considered in the model. Solid lines (—) indicate electron collisions (1: elastic, 2: excitation, 3: ionization), the dashed lines (---) indicate Ar^+ cross sections (4: isotropic part of elastic scattering, 5: backward elastic scattering, 6: excitation, 7: ionization), and the dotted lines (·····) indicate fast Ar atom cross sections (8: isotropic elastic scattering, 9: excitation, 10: ionization).

system. The energy sharing of the collision partners is determined from the scattering angles (see, e.g. [14]).

The cross section of the elastic $\text{Ar}^f + \text{Ar}$ collision in isotropic approximation is $Q_1^a = \left(\frac{3}{2}\right)Q_v$, where Q_v is the viscosity cross section [45]. The calculation of scattering angles and energy sharing is carried out in the same way as in the case of $\text{Ar}^+ + \text{Ar}$ collisions. The scattering of particles in inelastic heavy particle collisions is assumed to be isotropic in the COM system.

4. Experimental and theoretical data and their comparisons

4.1. Experimental results

The volt-ampere ($U-i$) characteristics of the discharges at pd values of 150, 75 and 45 Pa cm and for three different electrode gaps d are shown in figures 3(a)–(c). The discharge voltage is plotted as a function of scaling variable i/p^2 (where i is the discharge current). We used i/p^2 instead of j/p^2 (where j is the current density) since the effective discharge area is not easily determined for the constricted regime. (The proportionality $i \propto j$ is fulfilled only for the ‘one-dimensional’ diffuse abnormal mode of the discharge that occupies the entire area of the cathode.)

As we see in figure 3, at $pd = 150$ and 75 Pa cm the discharge voltage scales more or less with i/p^2 as expected for space-charge dominated discharges. At $pd = 75$ Pa cm, there is a systematic difference between voltage values for different electrode gaps, especially at higher currents (in normal and abnormal glow). However, these differences (the increase of voltage with increasing d) are small. On the other hand, for $pd = 45$ Pa cm the scaling does not hold, i.e. for the lowest pressures concerned here, electrical properties of the discharge strongly depend on the pressure and the electrode gap. There is a significant discrepancy between voltages for different electrode gaps at fixed values of i/p^2 in the range of normal glow and even more in the range of abnormal glow discharge.

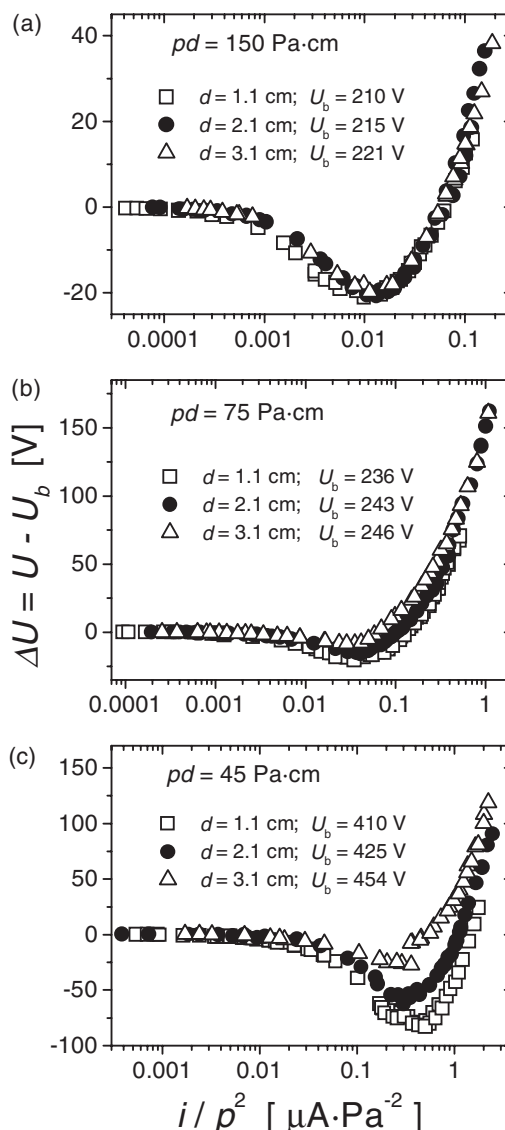


Figure 3. Volt-ampere characteristics of the discharge for different values of pd : (a) 150 Pa cm; (b) 75 Pa cm; (c) 45 Pa cm. The plots show the difference between actual discharge voltage (U) and breakdown voltage (U_b), as a function of the reduced discharge current i/p^2 . Different symbols correspond to the different values of electrode separation d .

The deviation of the $U-i/p^2$ characteristics in this domain of parameters is not attributed to the appearance of certain elementary processes that generally lead to the violation of scaling. (Such processes become gradually more important at increasing pressure due to their increased importance at higher densities, while we observe the violation of scaling at the lowest pressure.) Rather than that, the violation of scaling can be explained by the following two mechanisms, which become important at low pd values when the discharge tube diameter is kept constant (as in this experiment). (i) When the electrode separation becomes comparable to the diameter of the discharge, radial losses of charged particles become gradually more important. The discharge tries to enhance the ionization rate with the help of an increased voltage in order to compensate for the radial losses and to sustain a given current. (ii) Due to the specific electric field distribution around the

edges of the cathode, the spatial distribution of the ion flux to the cathode surface results in a decrease of the active area of the cathode (see, e.g. [5]). This reduction of the active cathode surface may be significant under low pd conditions, especially when the diameter/electrode separation ratio is small. This mechanism also results in an increase of the discharge voltage, as the current density over the active area is higher compared to a current density that would be uniformly distributed over the whole cathode area.

As will be shown later, the increased voltage leads to the appearance of heavy-particle processes. These processes—as they occur between fast ions or atoms and ground state background gas atoms—are also not expected to violate the scaling. (This, actually has also been tested in our simulations.) The reflection of fast electrons from the anode can modify the ionization rate in the discharge. This process may be important at low pd values (near/in the obstructed mode) but it also does not lead to violation of scaling as the flux-energy distribution of electrons before and after the reflection does scale.

For all the cases shown here, the data are in good agreement with the earlier measurements of electrical characteristics at lower currents and with the measurements of negative differential resistances [12].

Axial intensity profiles of light emission for selected values of current and for $pd = 150$ Pa cm, 75 Pa cm and 45 Pa cm are presented in figures 4–6, respectively. At the lowest currents considered here, we observe a continuous growth of emission towards the anode, corresponding to the Townsend regime. The spatial profiles of emission at such low currents have been studied in one of the previous papers [13]. These profiles clearly exhibit an exponential growth at very low currents. At somewhat higher currents, below the transition to the normal (constricted) glow, the growth can be described by a gradually changing exponent. With further current increase, the profile is consistent with the development of the cathode fall—the peak of emission gradually moves further from the anode, while the peak intensity increases. At the same time, emission profiles at $pd = 45$ Pa cm (figure 6) clearly exhibit the rising contribution of heavy-particle excitation through a peak close to the cathode [50, 51],—as the discharge pressure is lowered. This observation indicates that heavy-particle processes are sensitive on the discharge voltage, which is an increasing function of the electrode separation (see figure 3). Apart from observations under well-defined swarm conditions the emission close to the cathode (powered electrode) has been observed in glow and rf discharges many times [52] but very rarely has this emission been modelled.

In addition, under the usual assumption that the position of the negative glow peak coincides with the edge of the cathode-fall region [7], the present data allow us to determine the width of the cathode fall and to establish its dependence on current and pressure. Once more, we refer to the similarity principle and we observe that the scaling relation between pd_c (where d_c is the thickness of the cathode fall) and i/p^2 deviates in the range of lowest pressures covered here (see figure 7). At the lowest value of pd investigated (45 Pa cm) the length of the cathode sheath increases with increasing electrode gap. These results are consistent with the scaling properties of the discharge voltage observed in figure 3.

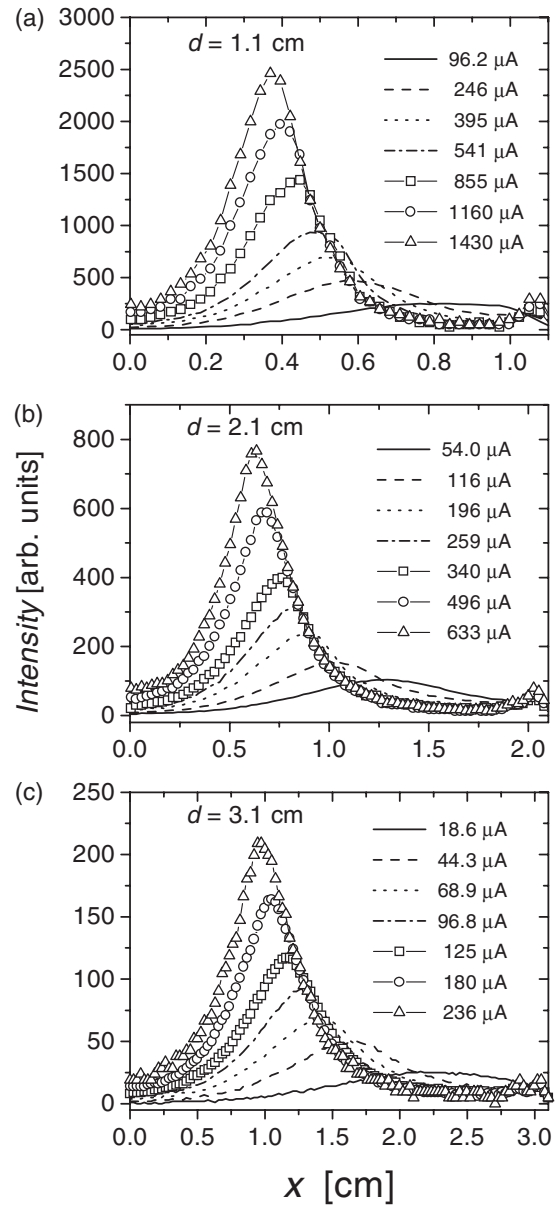


Figure 4. Axial profiles of emission at 150 Pa cm for three different values of d : (a) $d = 1.1$ cm; (b) $d = 2.1$ cm; (c) $d = 3.1$ cm. The cathode is situated at $x = 0$.

4.2. Simulation results and comparison with experimental data

In figure 8 we show a comparison between the model and the experimental light intensity distributions for $pd = 45$ Pa cm. One should bear in mind that the profiles are normalized only at one value of the current and the relative intensities are independent. First, we may observe that the light intensity peak close to the cathode increases as the discharge voltage increases (see figure 3) as E/N is increased. One observes only a small growth of excitation towards the cathode in the low current regime (Townsend discharge), so for higher currents the significant increase in E/N is required to induce the effect. This supports strongly the heavy-particle excitation as an explanation of the glow near the cathode, for which, actually the discharge simulations provide a direct evidence.

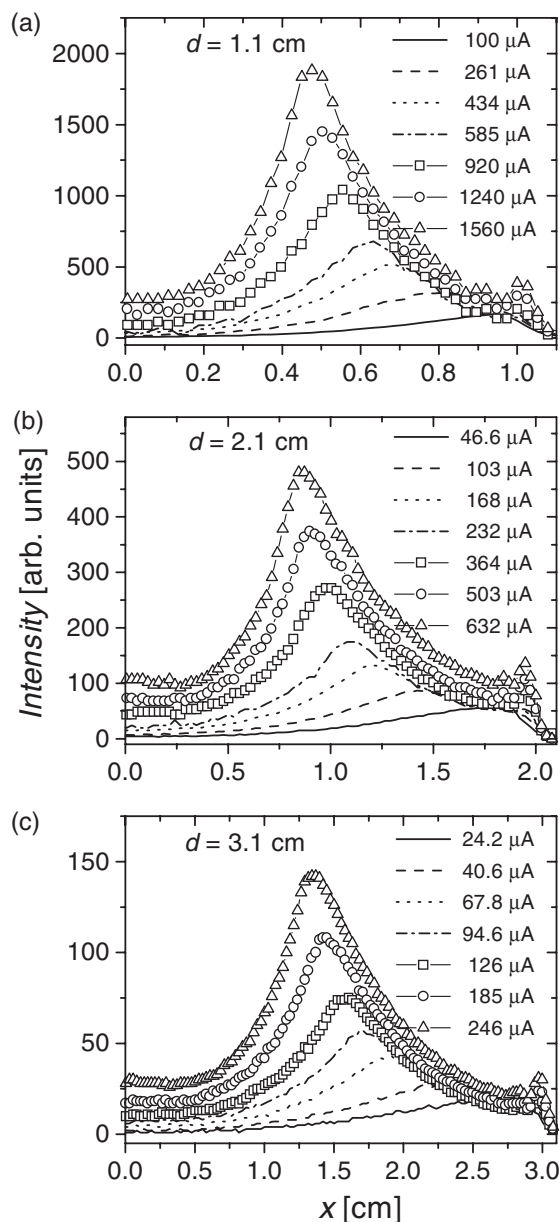


Figure 5. Axial profiles of emission at 75 Pa cm for three different values of d : (a) $d = 1.1$ cm; (b) $d = 2.1$ cm; (c) $d = 3.1$ cm. The cathode is situated at $x = 0$.

Spatial profiles obtained by the model that includes gas phase excitation are in very good agreement with experiments, having in mind uncertainties in the cross section data and limitations of the model.

At the higher pd values—as expected on the basis of the scaling of the experimental voltage–current characteristics—the measured and calculated light intensity curves are in even better agreement. For these conditions, heavy-particle excitation shows up only at the highest currents.

The excitation rate of Ar atoms is decomposed to contributions due to electron and heavy-particle impact in figure 9(a). Under these conditions, heavy-particle excitation plays an important role near the cathode. Similarly to the excitation processes, at high E/N values heavy-particle ionization also becomes important. The ‘additional’ electrons

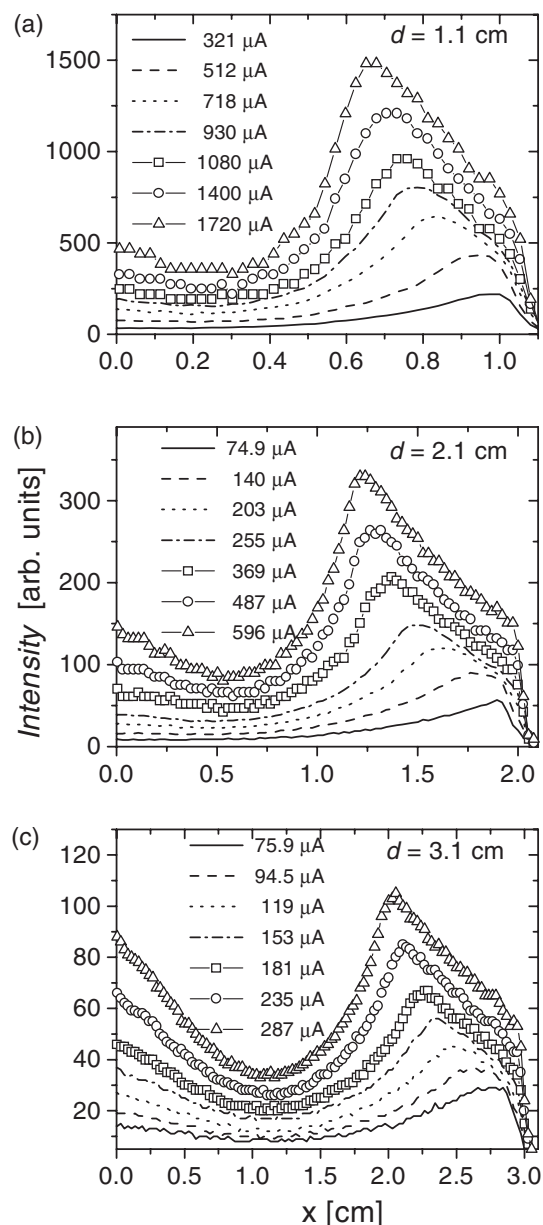


Figure 6. Axial profiles of emission at 45 Pa cm for three different values of d : (a) $d = 1.1$ cm; (b) $d = 2.1$ cm; (c) $d = 3.1$ cm. The cathode is situated at $x = 0$.

created via this process—as they are created near the cathode—behave almost like the electrons emitted from the cathode and have the potential to create further electron avalanches. This way the $\text{Ar}^f + \text{Ar}$ and $\text{Ar}^+ + \text{Ar}$ collisions greatly enhance the overall ionization and excitation rates. This is illustrated in figure 9(b) where the electron impact excitation rate is plotted as a result of the full simulation and in the case when heavy-particle processes are ‘artificially’ turned off in the simulation. The effect of heavy particle collisions on the electron impact excitation rate is remarkable under the conditions investigated, $pd = 45$ Pa cm, $d = 3.1$ cm and $U = 510$ V. Without including heavy-particle processes, the electron-impact excitation rate decreases by a factor of 3.

Charged particle creation via heavy-particle ionization partly compensates for the electron and ion losses to the wall

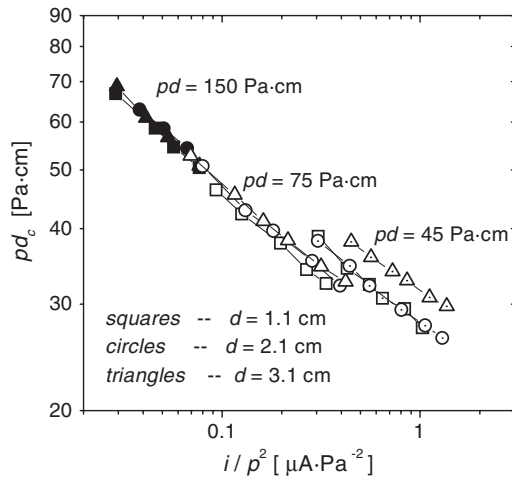


Figure 7. Width of the cathode fall d_c as a function of i/p^2 for three values of pd . Different symbols represent different electrode separations (d).

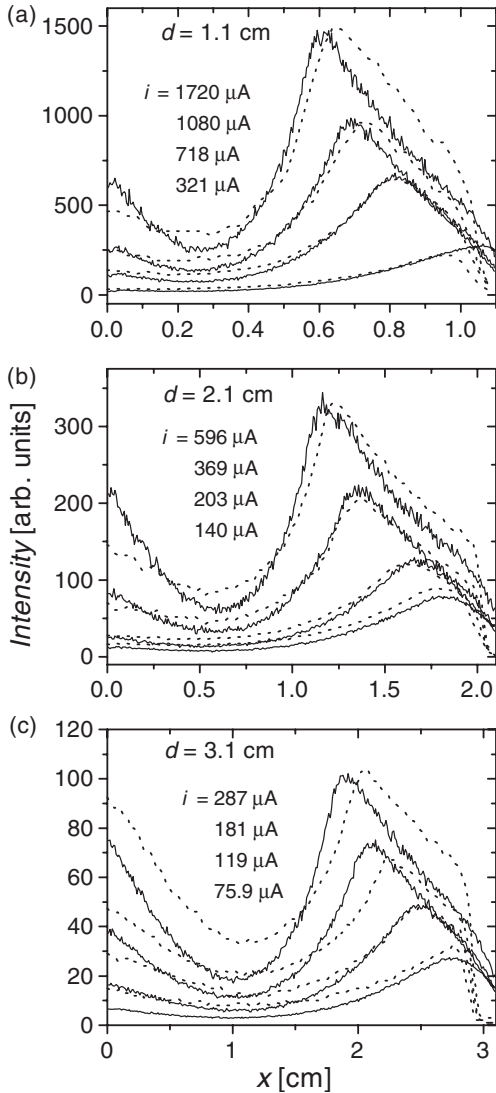


Figure 8. Comparison of experimental (---) and calculated (—) profiles of emission at 45 Pa cm: (a) $d = 1.1$ cm; (b) $d = 2.1$ cm; (c) $d = 3.1$ cm.

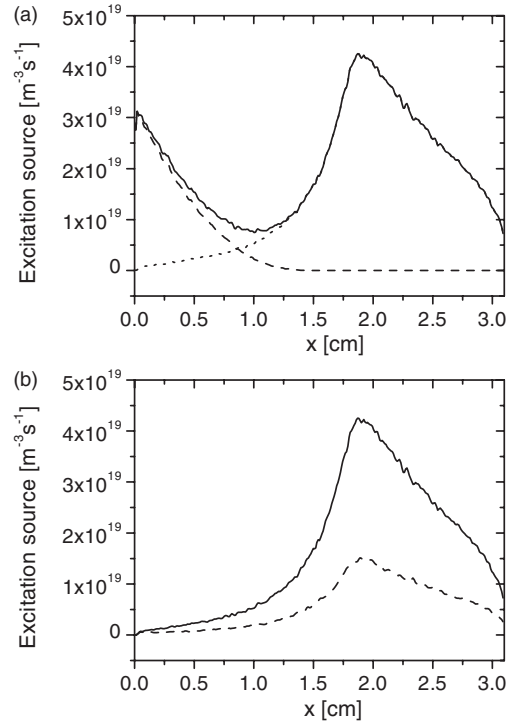


Figure 9. (a) Contributions of electron impact (·····) and heavy-particle impact (---) collisions to excitation of gas atoms, (—) total excitation rate. (b) Comparison of electron impact excitation profiles with (—) and without (---) heavy-particle processes being considered in the model, illustrating the effect of heavy-particle ionization on the electron flux. Discharge conditions: $pd = 45$ Pa cm, $d = 3.1$ cm.

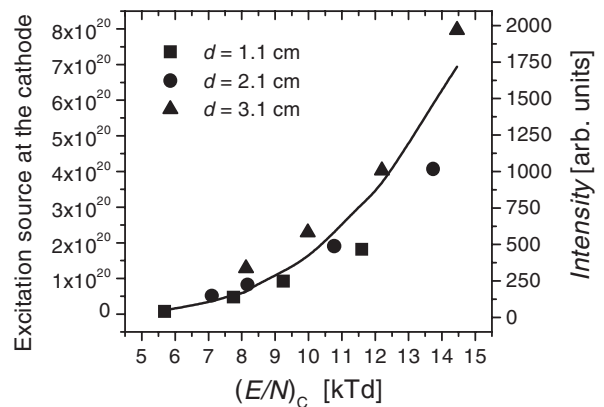


Figure 10. Normalized heavy-particle excitation rate near the cathode as a function of the reduced electric field at the cathode. The solid curve is a fit to the results of the simulation, the symbols indicate experimental data: $pd = 45$ Pa cm.

of the tube. The latter—being a loss mechanism—increases the discharge voltage, and this increase would be even more significant in the absence of heavy-particle processes.

The effectiveness of heavy-particle processes primarily depends on the strength of the reduced electric field E/N . This is illustrated in figure 10, where the normalized heavy-particle excitation rate $S^*(x)$ at the cathode is plotted against E/N at the cathode surface, $(E/N)_c$, for $pd = 45$ Pa cm. The excitation rate has been normalized by taking into account the dependence of current density on pressure (j/p^2 scaling) and

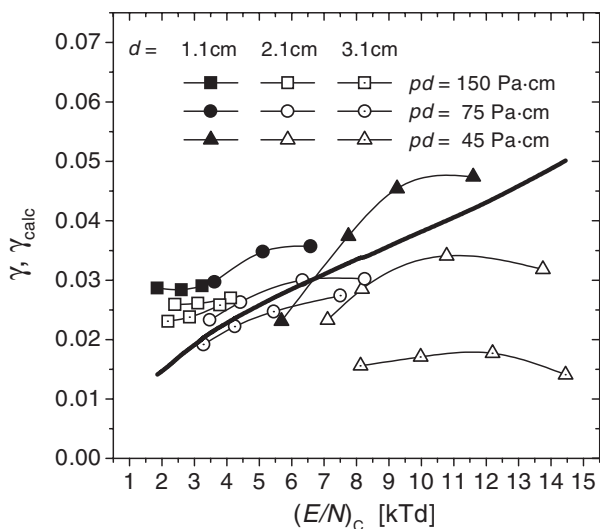


Figure 11. Fitted (γ , symbols) and calculated (γ_{calc} , heavy line) secondary electron yield values as a function of the reduced electric field at the cathode. In the case of γ_{calc} the values fall on a universal curve.

the length scaling in similar discharges. The data obtained from the simulation of the discharges with different electrode separations show a universal behaviour independent of the electrode separation. The experimental data (peak intensities) agree well with the simulation results. The excitation rate exhibits a strong nonlinear dependence on E/N .

The apparent secondary yield (γ) values resulting from the fitting of the calculated and measured currents are plotted in figure 11 as a function of the reduced electric field at the cathode $(E/N)_c$. These values closely follow a universal curve for the different pd and d values. The figure also shows the values obtained from the flux-energy distribution of heavy particles, γ_{calc} , calculated according to equation (3.1). Taking into account the uncertainties of the particle-induced secondary yield data, the agreement between the two sets of γ values is acceptable. At the highest pd (150 Pa cm) the fitted γ values are above the calculated values. Besides the above-mentioned uncertainties of the input data, this difference may be attributed to the simplifications of the model: in equation (3.1) we neglected the contributions of metastable atoms and photons to secondary electron emission at the cathode. At the intermediate pd of 75 Pa cm a better agreement is obtained, while a gradually developing discrepancy appears again at 45 Pa cm, with increasing electrode separation. The fitting procedure results a γ that is significantly smaller than that corresponding to a one-dimensional situation (corresponding to the γ value determined from equation (3.1)). At such conditions the reduction of the active cathode area [5] becomes significant. As a consequence of this, the discharge current is much smaller than jA_{cathode} , where j is the current density at the active (inner) part of the cathode surface. The decreased current (average current density) is established by a decreased γ in the one-dimensional model.

5. Summary

In this paper, we reported investigations of electrical characteristics and light intensity distributions of argon glow

discharges in the abnormal mode, where excitation and ionization processes by fast heavy particles (Ar^+ and Ar^f) are important. We found that the scaling of current with electrode separation is obeyed at higher pd values, but discrepancies occur at low pd conditions. Two mechanisms: (i) the radial losses of charged particles; and (ii) the reduction of the active cathode area were identified as the main reasons for the violation of the $U = f(i/p^2)$ scaling [4, 5]. Both of these mechanisms become important when the electrode separation becomes comparable to the tube diameter, and are responsible for the increase of the discharge voltage. Heavy-particle ionization—which appears at the highest voltages covered here—can only partially compensate for these mechanisms. The violation of the scaling laws also showed up in the length of the cathode sheath. While at high pd the length of the cathode sheath d_c depended only on i/p^2 , at low pd a dependence of d_c on the electrode separation, d , was also observed.

The occurrence of heavy-particle processes was identified experimentally by observing the cathode glow—light emission near the cathode due to $\text{Ar}^f + \text{Ar}$ collisions. These simulation studies, complementing the experimental work, yielded spatial light intensity distributions in good agreement with the experimental data, including heavy-particle excitation. The simulations also indicate that heavy-particle ionization processes contribute significantly to the ionization balance of the discharge and that the conditions where heavy-particle contribution is significant coincide with the breakdown of scaling. The breakdown of scaling, however, should not be attributed to the heavy-particle processes themselves, as these processes are ‘linear’ in the sense that they occur between fast species and ground state buffer gas atoms, unlike, e.g. recombination or metastable–metastable collisions. The rates of these processes depend on E/N , more precisely on its spatial distribution, $E(x/d)/N$, in the discharge gap. Thus, in similar discharges, where the $E(x/d)/N$ distribution is the same, heavy-particle processes should have the same effect.

This study may be used as a test case for learning how to model the secondary electron production at the surface and in the gas phase by heavy particles, which is required to achieve fully self-consistent models of non-equilibrium plasmas.

Acknowledgments

This work has been supported by the project MNTRS 1478, SANU and the Hungarian Scientific Research Fund (OTKA-T-34156).

References

- [1] Petrović Z Lj and Phelps A V 1993 *Phys. Rev. E* **47** 2806
- [2] Phelps A V, Petrović Z Lj and Jelenković B M 1993 *Phys. Rev. E* **47** 2825
- [3] Phelps A V and Petrović Z Lj 1999 *Plasma Sources Sci. Technol.* **8** R21
- [4] Lisovskiy V A, Yakoven S D and Yegorenkov V D 2000 *J. Phys. D: Appl. Phys.* **33** 2722
- [5] Donkó Z, Bánó G, Szalai L, Kutasi K, Rózsa K, Pinheiro M and Pinhão N 1999 *J. Phys. D* **32** 2416
- [6] Phelps A V, Pitchford L C, Pédoussat C and Donkó Z 1999 *Plasma Sources Sci. Technol.* **8** B1
- [7] Marić D, Kutasi K, Malović G, Donkó Z and Petrović Z Lj 2002 *Eur. Phys. J. D* **21** 73

- [8] Phelps A V 2001 *Plasma Sources Sci. Technol.* **10** 329
- [9] Donkó Z 2001 *Phys. Rev. E* **64** 026401
- [10] Boeuf J P and Pitchford L C 1995 *J. Phys. D: Appl. Phys.* **28** 2083
- [11] Hartmann P, Donkó Z, Bánó G, Szalai L and Rózsa K 2000 *Plasma Sources Sci. Technol.* **9** 183
- [12] Stefanović I and Petrović Z Lj 1997 *Japan. J. Appl. Phys.* **36** 4728
- [13] Živanov S, Živković J, Stefanović I, Vrhovac S and Petrović Z Lj 2000 *Eur. Phys. J. Appl. Phys.* **11** 59
- Živanov S, Živković J, Stefanović I, Vrhovac S and Petrović Z Lj 1995 *J. Phys. D: Appl. Phys.* **28** 2083
- [14] Bogaerts A, van Straaten M and Gijbels R 1995 *Spectrochim. Acta* **50B** 179
- [15] Bogaerts A and Gijbels R 1995 *J. Appl. Phys.* **78** 6427
- [16] Bogaerts A, Donkó Z, Kutasi K, Bánó G, Pinhão N and Pinheiro M 2000 *Spectrochim. Acta (part B)* **55** 1465
- [17] Bogaerts A and Gijbels R 1995 *Phys. Rev. A* **52** 3743
- [18] Bogaerts A, Gijbels R and Goedheer W J 1996 *Anal. Chem.* **68** 2296
- [19] Bogaerts A 1999 *Plasma Sources Sci. Technol.* **8** 210
- [20] Shidoji E, Ohtake H, Nakano N and Makabe T 1999 *Japan. J. Appl. Phys.* **38** 2131
- [21] Shidoji E, Nakano N and Makabe T 1999 *Thin Solid Films* **351** 37
- [22] Shidoji E, Ness K and Makabe T 2001 *Vacuum* **60** 299
- [23] Donkó Z 2000 *J. Appl. Phys.* **88** 2226
- [24] Donkó Z 2001 *Phys. Rev. E* **64** 026401
- [25] Pitchford L C, Boeuf J P, Segur P and Marode E 1990 *Nonequilibrium Effects in Ion and Electron Transport* ed J W Gallagher (New York: Plenum)
- [26] Sakai Y, Tagashira H and Sakamoto S 1977 *J. Phys. D: Appl. Phys.* **10** 1035
- [27] Boeuf J P and Marode E 1982 *J. Phys. D* **15** 2169
- [28] Tagashira H, Sakai Y and Sakamoto S 1977 *J. Phys. D: Appl. Phys.* **10** 1051
- [29] Winkler R, Petrov G, Sigenege F and Uhrlandt D 1997 *Plasma Sources Sci. Technol.* **6** 118
- [30] Uhrlandt D, Schmidt M, Behnke J F and Bindemann T 2000 *J. Phys. D: Appl. Phys.* **33** 2475
- [31] Hannemann M, Hardt P, Loffhagen D, Schmidt M and Winkler R 2000 *Plasma Sources Sci. Technol.* **9** 387
- [32] Ferreira C M and Loureiro J 2000 *Plasma Sources Sci. Technol.* **9** 528
- [33] Porokhova I A, Golubovskii Yu B, Bretagne J, Tichy M and Behnke J F 2001 *Phys. Rev. E* **63** 056408
- [34] Fiala A, Pitchford L C and Boeuf J P 1994 *Phys. Rev. E* **49** 5607
- [35] Boeuf J P and Pitchford L C 1991 *IEEE Trans. Plasma Sci.* **19** 286
- [36] Bogaerts A and Gijbels R 2002 *Plasma Sources Sci. Technol.* **11** 27
- [37] Kutasi K and Donkó Z 2000 *J. Phys. D* **33** 1081
- [38] Kutasi K, Hartmann P and Donkó Z 2001 *J. Phys. D* **34** 3368
- [39] Hartmann P, Matsuo H, Otsuka Y, Kando M and Donkó Z 2003 *Japan. J. Appl. Phys.* **42** 3633
- [40] Boeuf J P and Pitchford L C 1991 *IEEE Trans. Plasma Sci.* **19** 286
- [41] Revel I, Pitchford L C and Boeuf J P 2000 *J. Appl. Phys.* **88** 2234
- [42] Hagstrum H D 1953 *Phys. Rev.* **89** 252
- [43] Thomas S and Pattison E B 1970 *J. Phys. D* **3** 349
- [44] Thomas E W 1985 *Oak Ridge Nat. Lab. Report ORNL-6088/V3, E-10*
- [45] Phelps A V *Collision Data Compilation* ftp://jila.colorado.edu/collision_data
- [46] Phelps A V 1991 *J. Phys. Chem. Ref. Data* **20** 557
- [47] Phelps A V 1994 *J. Appl. Phys.* **76** 747
- [48] Yoshida S, Phelps A V and Pitchford L C 1983 *Phys. Rev. A* **27** 2858
- [49] Opal C B, Peterson W K and Beaty E C 1971 *J. Chem. Phys.* **55** 4100
- [50] Phelps A V and Jelenković B M 1988 *Phys. Rev. A* **38** 2975
- [51] Petrović Z Lj and Stojanović V 1998 *J. Vac. Sci. Technol. A* **16** 329–36
- [52] Mutsukura N, Kobayashi K and Machi Y 1989 *J. Appl. Phys.* **66** 4688–95
- Wild Ch, Wagner J and Koidl P 1987 *J. Vac. Sci. Technol. A* **5** 2227–30